2023 IEEE International Conference on Systems, Man, and Cybernetics (SMC)
October 1-4, 2023, Oahu, Hawaii, USA

2D Ultrasound-guided Visual Servoing for In-plane Needle Tracking in Robot-Assisted Percutaneous Nephrolithotomy

Hoorieh Mazdarani
Systems and Computer Engineering
Carleton University
Ottawa, Canada
hooriehmazdarani@cmail.carleton.ca

Alec Cotton
Systems and Computer Engineering
Carleton University
Ottawa, Canada
aleccotton@cmail.carleton.ca

Carlos Rossa
Systems and Computer Engineering
Carleton University
Ottawa, Canada
rossa@sce.carleton.ca

***Abstract*—Ultrasound (US)-guided percutaneous nephrolithotomy is a surgical procedure for large kidney stone removal through an incision in the patient's back. To gain kidney access, the surgeon steers a needle towards the kidney while simultaneously controlling the position and orientation of a US probe to keep the needle in the image plane. To successfully reach the kidney while avoiding delicate structures, a significant level of skill and precision is required. To alleviate the surgeon's cognitive workload, robot-assisted needle tracking can be implemented to autonomously track the needle in the US images and adjust the US probe's position and orientation such that the same portion of the needle is visible in the images.**

This paper presents a US-guided visual servoing (VS) algorithm to track the translation and rotation of a needle in a plane. Image features representing the desired pose of the needle in the image are defined, through which an interaction matrix is devised to relate the rate of the change of the image features in US images to the required position and orientation of the US probe connected to a robotic manipulator. Experimental results in 4 experimental scenarios in a water tank demonstrate the capability of the proposed method in tracking the needle in real-time with an accuracy of 2.6 mm with a control rate of 20 Hz. Although VS has been used to track surgical targets in the past, this paper proposes the first implementation of VS for needle tracking in longitudinal US images subjected to 3-DOF motion in a plane without any prior knowledge of needle trajectory or additional position sensors.

***Index Terms*—Medical robotics, ultrasound imaging, visual servoing, needle tracking, percutaneous nephrolithotomy, ultrasound guidance, biomedical imaging.**

I. Introduction

Percutaneous nephrolithotomy (PCNL) is the gold standard surgical treatment for large upper urinary tract calculi. In PCNL, the surgeon makes a small incision in the patient's back and inserts a small calibre tube to access the kidney. An endoscope is then passed down the tube into the kidney to fragment and remove the kidney stones. Despite over 40 years of development, PCNL has a steep learning curve and is associated with a high risk of complications such as bleeding, renal pelvis perforation, and colon and spleen injuries [1].

Kidney access during PCNL may be performed using different imaging modalities, including fluoroscopy, ultrasound (US), or a combination of both. Fluoroscopy has been the preferred modality for kidney access in North America, however, it exposes both patients and medical professionals to significant levels of radiation [2]. Moreover, fluoroscopy only allows for single-plane imaging, making accurate kidney puncture challenging. Organs adjacent to the kidney such as the pleura and the bowels are not visible during puncture, posing the risk of accidental injury [3]. US-guided PCNL (usPCNL) is the main alternative to fluoroscopy. US can detect radiolucent stones, improve visualization of adjacent viscera, and gives a clearer delineation of the anterior and posterior calyces in a radiation-free setting [4]. However, usPCNL requires an advanced level of dexterity to guide the needle toward the stones while keeping it visible in the US image.

US-guided kidney access can be performed using longitudinal or transverse images. In longitudinal imaging, the needle appears as a line in the US image. The surgeon must precisely coordinate the hand holding the US probe and the hand holding the needle to keep the needle shaft aligned with the imaging plane, while simultaneously visualizing the target. If the needle tip is not visible in the image, the surgeon may inadvertently puncture the surrounding organs. In transverse imaging, the needle shaft is perpendicular to the imaging plane and, therefore, the needle shaft is not visible in the image. To guide the needle tip toward the target the surgeon constantly adjusts the imaging plane by sweeping the probe back and forth along the needle. In both modalities, parts of the kidney are shadowed by the ribs, which further complicates the procedure [5]. These complications are exacerbated by potential misinterpretation of US images and lack of training, often leading to inaccurate needle placement [1] and create a steep learning curve with as few as 11% of urologists being able to achieve kidney access themselves [2].

To alleviate the surgeon's cognitive workload and the complexity of usPCNL, one may consider methods to reduce the

We acknowledge the support of the Natural Sciences and Engineering Research Council of Canada (NSERC), [funding reference number 2018-06074]. Cette recherche a été financée par le Conseil de recherches en sciences naturelles et en génie du Canada (CRSNG), [numéro de référence 2018-06074].

level of technical skills required to perform it. For example, a needle guide may be used to help keep the needle in the US imaging plane at the cost of limited dexterity [5]. Some have considered augmented reality to help steer the needle toward the calix [6], [7], while others have focused on robotic assistance to facilitate kidney access [8], [9]. A common aspect of these methods is the need to determine the position and orientation of the needle in the images. For example, Chen et al. [10] propose a neural network for needle detection that uses a longitudinal and an orthogonal image to estimate the needle pose in 3D. In [11], the concept is taken one step further: optical flow is used to segment a cannula from 2D-US images and translate the probe using a robotic arm in predefined intervals to keep the needle centred in the image. In [12] a robotic arm autonomously translates and orients the US probe along a pre-defined needle trajectory. However, during manual needle steering the position and orientation of the needle are not known beforehand. Real-time adjustments to the US probe position and orientation are therefore required to ensure continuous visualization of the needle in the image.

A solution to the limitations highlighted above can be sought in visual servoing (VS) - a technique employed to control the motion of a robot through visual information obtained from a camera or a sensor. Its primary benefit is the ability to accurately control the robot's pose relative to an image target or feature. For example, in [13], VS is combined with US imaging to position a robot-actuated needle in the image plane during percutaneous cholecystectomy. Haxthausen et al. [14] show the feasibility of using VS with 2D US for semi-automated scanning of peripheral arteries. In [15], model-free VS is used to actuate a robot-controlled US probe to image a desired cross-section of a static target. Nadeau et al. [16] use graph-cut segmentation of three orthogonal US images to extract image features from a target. A robot arm then controls the in-plane motion of the US probe in the three orthogonal image planes to image the target. In all these examples, the position of the US probe is controlled to image a static target, that is, VS is used for autonomous imaging rather than for real-time tracking. However, during usPCNL the target (i.e., the needle) moves relative to the probe as the needle is steered toward the kidney. While 3D US images may be used to track the moving needle, 3D US is more complex than 2D, has a much lower frame rate, and may not be suitable for real-time needle steering [17], [18].

This paper proposes a new US-based VS algorithm for longitudinal needle tracking using only 2D-US images. It accounts for needle motion in 3 degrees-of-freedom (3-DOF), that is, two in-plane translations and one in-place rotation. In the proposed approach, the US probe is attached to a robotic manipulator that is controlled to follow the 3-DOF motion of the needle in a plane. This is accomplished by defining a longitudinal image having the desired position and orientation of the needle. Image features are then extracted from both the desired image and real-time US images. Based on the error between them, the algorithm determines the required linear and angular speed of the US probe that minimize the difference between the desired and current image features. This ensures that the needle shaft is always visible in the images as the needle moves in a fixed plane. In contrast to the algorithms described earlier, needle tracking is achieved in 3-DOF and without any prior knowledge about the needle trajectory. The method is computationally efficient and well-suited for real-time needle steering. To the best of the author's knowledge, this paper proposes the first VS method for tracking a moving needle using longitudinal US images with 3-DOF. This is a crucial first step toward automating kidney access during usPCNL procedure with real-time US image feedback.

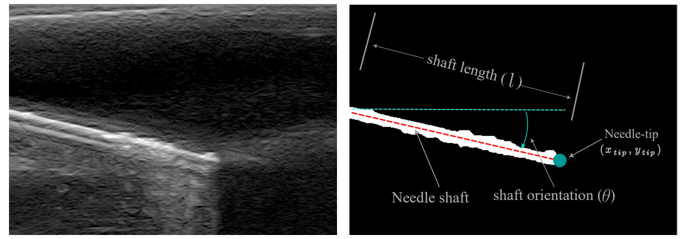

Fig. 1. (a) Longitudinal US image of a needle in a water tank; (b) Binary image of the needle showing the features used in the VS algorithm, i.e., the shaft length ℓ, the Cartesian position of the needle tip in the image (x_{tip}, y_{tip}), and the needle shaft orientation θ.

The paper is organized as follows. Section 2 introduces the proposed VS algorithm, the image features, and the robot control law. The experimental setup is presented in Section 3. The US probe is connected to a robot arm and a second robot is used to move the needle. While in usPCNL the surgeon performs the needle steering, the second robot used in this paper provides measurable movements to validate the accuracy of the proposed algorithm. The needle and probe are submerged in a water container so that both the needle and probe can be moved freely. The feasibility of the proposed method in in-plane needle tracking is then demonstrated for 4 different test scenarios in Section 4. Finally, in Section 5 a discussion of the obtained results and recommendations for future work are presented.

II. Visual Servoing for In-Plane Needle Imaging

Using longitudinal US images the surgeon must precisely coordinate the position and orientation of the US probe so that the needle shaft and the needle tip are visible at all times. As the needle is advanced towards a target, the objective is to maintain a constant needle pose in the US image.

The principle of US-based VS is to attach the probe to a robot and move the robot to follow the motion of the needle. The first step in the algorithm is to define a desired/target US image and select appropriate features from both the desired and real-time images that are time-variant and differentiable. Fig. 1(a) shows a longitudinal sample image of the needle and Fig. 1(b) shows the main features that can be associated with it, including the needle length in the image ℓ, the position of the needle tip in the image (x_{tip}, y_{tip}), and the orientation of the needle shaft with respect to the US probe horizontal axis θ. The choice of these features is essential to ensure appropriate performance of the robot controller, which must guarantee that visual features extracted from the image converge to the desired values [19]. This section details how these main features are calculated in a 2D US image, and then formulates an interaction matrix that relates the visual features' time variation to the robot's end-effector velocities, i.e., the velocity of the probe in 3-DOF. The interaction matrix is then employed to design the VS controller.

A. Visual Features Definition

In a 2D image, features can be defined in terms of moments of different orders. The general form for image moment of order $i+j$ in a grayscale image is defined as:

$$m_{ij} = \iint x^i y^j I(x,y) dx dy, \tag{1}$$

where (x,y) are the coordinates of the image pixel and $I(x,y)$ is the intensity of each pixel. Like other VS applications, only the shape of the object is important, i.e., the needle's cross-section. Thus, a binary threshold image segmentation algorithm can be used to segment the needle from the US image. Therefore, $I(x,y) = 1$ within the object's contour (indicated by $\mathcal{S}$), and $I(x,y) = 0$ over the rest of the pixels in the images. Thus, (1) simplifies to:

$$m_{ij} = \iint_{\mathcal{S}} x^i y^j dx dy. \tag{2}$$

With a digital image, the double integral can be replaced by a discrete sum defined as:

$$m_{ij} = \sum_{\mathcal{S}} x^i y^j \tag{3}$$

The features representing the needle in the US image defined in Fig. 1(b) can be written in terms of moments of orders up to two. The position of the needle tip in the image is:

$$\begin{aligned} x_{tip} &= l \cos\theta \\ y_{tip} &= \frac{m_{01}}{m_{00}} + \frac{1}{2} l \sin\theta. \end{aligned} \tag{4}$$

The needle shaft orientation with respect to the horizontal imaging axis is:

$$\theta = \frac{1}{2} \arctan\left(\frac{2\mu_{11}}{\mu_{20} - \mu_{02}}\right), \tag{5}$$

and the length of the needle shaft in the image is given by

$$l = 4\sqrt{\frac{2}{m_{00}}\left(\mu_{20} + \mu_{02} + \sqrt{(\mu_{20} - \mu_{02})^2 + 4\mu_{11}^2}\right)} \tag{6}$$

where

$$\begin{aligned} \mu_{11} &= m_{11} - \tfrac{m_{10} m_{01}}{m_{00}} \\ \mu_{20} &= m_{20} - \tfrac{m_{10}^2}{m_{00}} \\ \mu_{02} &= m_{02} - \tfrac{m_{01}^2}{m_{00}}. \end{aligned}$$

A vector containing all image features can now be defined as

$$\mathbf{s} = [x_{tip} \quad y_{tip} \quad \theta \quad l]^T \tag{7}$$

It should also be noted that the image moments are defined in the image frame, which coincides with the US probe frame.

B. Interaction Matrix Definition

The next step in the algorithm is to define a matrix L_s that relates the temporal variation of the image features, that is the first derivative of (7) with respect time $\dot{\mathbf{s}}$, to the speed of the US probe, so that:

$$\dot{\mathbf{s}} = \mathrm{L}_s \mathbf{v} \tag{8}$$

where $\mathrm{L}_s \in \mathbf{R}^{4\times 3}$ is the interaction matrix and $\mathbf{v} = [v_x \quad v_y \quad \omega_z]^T$ is a vector containing the translational velocity of the probe on the needle's imaging plane, and the angular velocity of the probe about an axis perpendicular to that plane.

The time variation of image features in terms of probe velocities can be written as:

$$\dot{\mathbf{s}}_i = \frac{\partial \mathbf{s}_i}{\partial v_x} v_x + \frac{\partial \mathbf{s}_i}{\partial v_y} v_y + \frac{\partial \mathbf{s}_i}{\partial \omega_z} \omega_z \tag{9}$$

In order to calculate the partial derivatives in (9), the common approach is to use the time variation of image moments in (2) in terms of probe velocities, and then using (4)-(6) to find $\dot{\mathbf{s}}$. However, in this application, the geometrical interpretation of image features is used instead. The time variation of image features is given directly as:

$$\begin{cases} \dot{x}_{tip} = -v_x + (l \sin\theta + \epsilon \cos\theta)\omega_z \\ \dot{y}_{tip} = -v_y - (x_{tip} - \epsilon \sin\theta)\omega_z \\ \dot{\theta} = -\omega_z \\ \dot{l} = -(\sqrt{1 + \sin^2\theta}) v_x + \epsilon \omega_z \end{cases} \tag{10}$$

where $0 < \epsilon \ll 1$. Finally, the interaction matrix relating the time derivatives of the image features with the probe velocity can be written as:

$$\mathrm{L}_s = \begin{bmatrix} -1 & 0 & l\sin\theta + \epsilon\cos\theta \\ 0 & -1 & -x_{tip} + \epsilon \sin\theta \\ 0 & 0 & -1 \\ -\sqrt{1+\sin^2\theta} & 0 & \epsilon \end{bmatrix} \tag{11}$$

C. Robot controller design

A classic control law widely used in VS determines the control action, i.e., the velocity of the US probe, based on the error observed between the desired features $\mathbf{s}^*$ and the actual time-variant image features $\mathbf{s}(t)$ calculated on the real-time US images. Defining the error signal as $\mathbf{e}(t) = \mathbf{s}^* - \mathbf{s}(t)$, the VS control law to minimize the features' error is:

$$\mathbf{v_c} = \mathbf{k_p} \mathbf{L_s}^{\dagger} (\mathbf{s}^* - \mathbf{s}) \tag{12}$$

where $\mathbf{v_c}$ is the probe's velocity (i.e., the robot end-effector's velocity), $\mathbf{k_p} \in R^{3\times 3}$ is a diagonal matrix including positive control gains, and $\mathbf{L_s}^{\dagger}$ is the pseudo-inverse of the estimated interaction matrix ($\mathbf{L_s}$) calculated at each sample, which is given by:

$$\mathbf{L_s}^{\dagger} = \mathbf{L_s}^T \left(\mathbf{L_s} \mathbf{L_s}^T\right)^{-1} \tag{13}$$

When using a correct estimation of $\mathbf{L_s}$, the closed-loop system is locally asymptotically stable [15]. Here, the desired feature vector $\mathbf{s}^*$ represents the desired cross-section image of the needle, which in turn defines the desired pose of the robot arm holding the US probe. A block diagram of the proposed

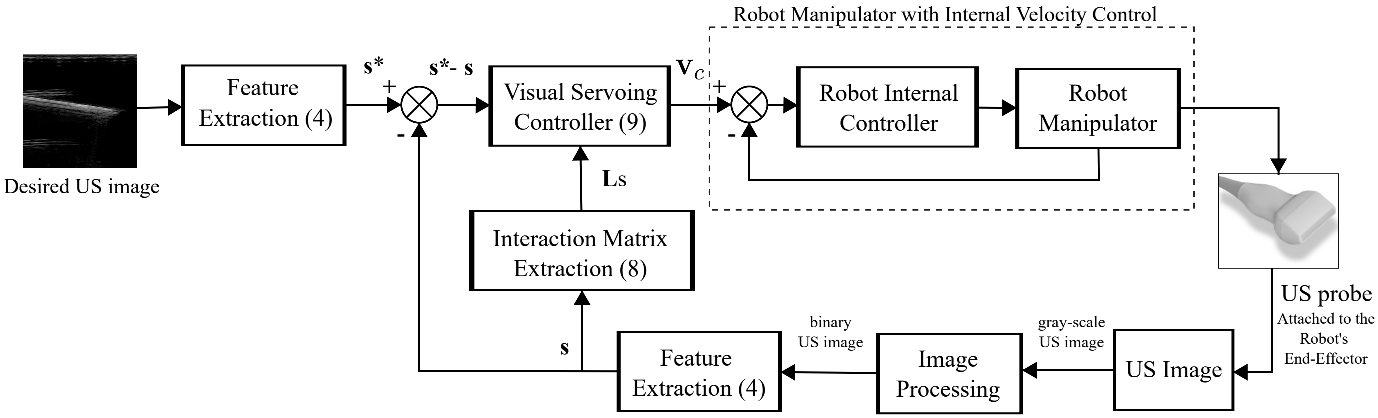

Fig. 2. Block diagram of the proposed algorithm. Image features extracted from a desired US image and from real-time US image are multiplied by a time-variant interaction matrix to determine the required speed of the US probe that makes the current feature tend to the desired image features.

needle tracking method is shown in Fig. 2. As discussed earlier, a simple image processing algorithm is applied to the US image to segment the needle and provide a binary image to be used in the feature extraction algorithm.

III. Experimental procedure

In order to implement and validate the proposed method, the experimental setup shown in Fig. 3 is used. In this configuration, a 40-mm wide US probe (L15-7H40-A5 from Telemed Ultrasound, Vilnius, Lituania) is attached to the end-effector of 6-DOF robot arm (Meca500 from Mecademic, Montréal, Canada) to image a 16-gauge needle. The US probe communicates with an ArtUs Telemed US machine and streams images in real-time at 50 Hz according to the specifications given in Table I. In this paper, both the needle and the US probe are submerged in a water tank to allow the needle to move freely. In percutaneous surgeries, needle steering is typically performed manually. However, in this paper, a second robot manipulator controls needle movement in the water tank, so that the motion of the needle and the corresponding motion of the US probe can be measured and compared.

For longitudinal, in-plane needle tracking, it is assumed that the needle moves on a fixed plane and rotates about an axis normal to that plane, that is, it has translational velocities υ_x, υ_y, and angular velocity ω_z. The features vector therefore is $\mathbf{s} = [x_{tip} \quad y_{tip} \quad \theta \quad l]^T$. The interaction matrix $\mathbf{L_s}$ is calculated assuming $\epsilon = 0.01$, and the proportional control gain is set to $\mathbf{k_p} = \text{diag}(0.5, 0.5, 0.2)$. Binary threshold image segmentation is applied to real-time US images to generate the images that serve as the input to the image moments defined (2), exactly as shown in Fig. 1b.

The algorithm is implemented on an Intel(R) Core i7-9700K computer with a 3.60 GHz CPU and 64GB of RAM. Matlab is used for both US image acquisition and robot control, with a sampling rate of 20 Hz. Once the needle is positioned in the water tank, the robot holding the US probe is moved manually until the needle becomes visible in the US images. The target image and target image features are extracted from Fig. 1b. As

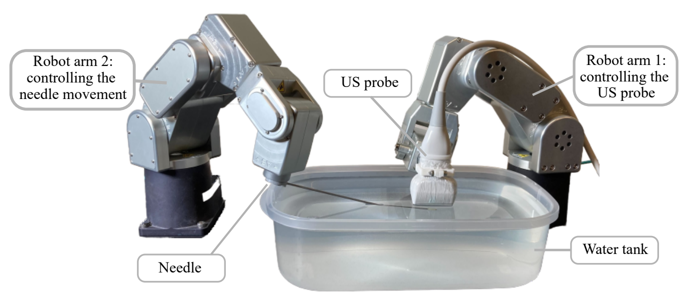

Fig. 3. Experimental setup. The needle and the US probe are each connected to a robot arm and submerged in a water tank. As robot 2 moves the needle in a random sequence in a plane, robot 2 adjusts the position and orientation of the US to minimize the error between the desired and actual image features.

TABLE I
Ultrasound image acquisition parameters

frequency	gain	focus	depth	dyn. range	power
10 MHz	79 %	14-21 mm	30 mm	72 dB	-4 dB

one robot moves the needle in the water tank, the controller is started to autonomously move the US probe so that the target image is maintained, based solely on the US images and VS algorithm.

To validate the feasibility of the proposed method, 4 test scenarios that simulate real needle steering procedures in usPCNL, are used:

- **Scenario 1**: The needle base is moved on a horizontal path along the x-axis with a constant linear speed of $\upsilon_x = 4$ mm/s (with $\upsilon_y = \omega_z = 0$).
- **Scenario 2**: The needle base is moved on a straight line in the $x - y$ plane with constant linear speeds of $\upsilon_x = 4$ mm/s and $\upsilon_y = -1$ mm/s (with $\omega_z = 0$).
- **Scenario 3**: The needle shaft orientation around the z-axis is changed with a constant angular velocity of $\omega_z = -0.6$ deg/s so that the needle tip follows a curved path in the $x - y$ plane.

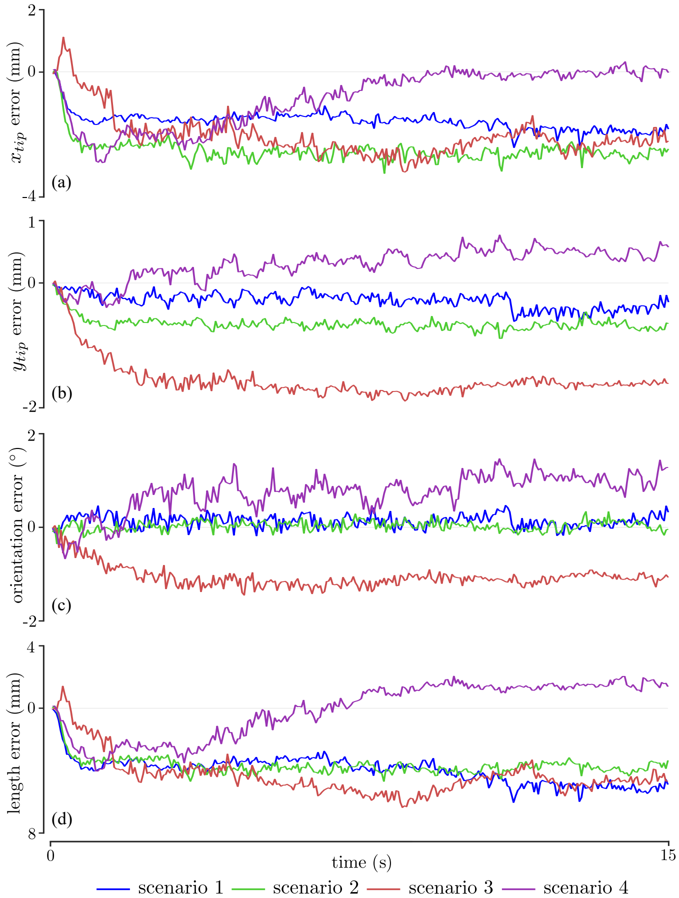

Fig. 4. Calculated error between desired and actual image features during VS-based tracking for x_{tip}, y_{tip}, θ, and l in each experimental scenario.

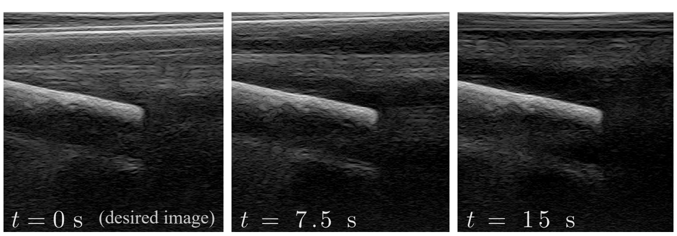

Fig. 5. US image of the needle during the tracking procedure in Scenario 4.

- **Scenario 4**: The needle base is moved on a path with constant linear and angular velocities $\upsilon_x = 4$ mm/s, $\upsilon_y = -2$ mm/s, and $\omega_z = 0.6$ deg/s.

These 4 scenarios are run for 15 seconds with a sampling time of 50 ms. The feature error along with the position of each robot arm is then evaluated.

IV. Results and Discussion

Fig. 4 shows the calculated feature error in each scenario. Despite the needle displacement, the US image remains stable, with less than a 3 mm error in the needle tip position and less than 1.5° error in the shaft orientation with respect to the desired pose. These errors are sufficiently small to have a negligible effect on the US images, as can be seen in Fig. 5.

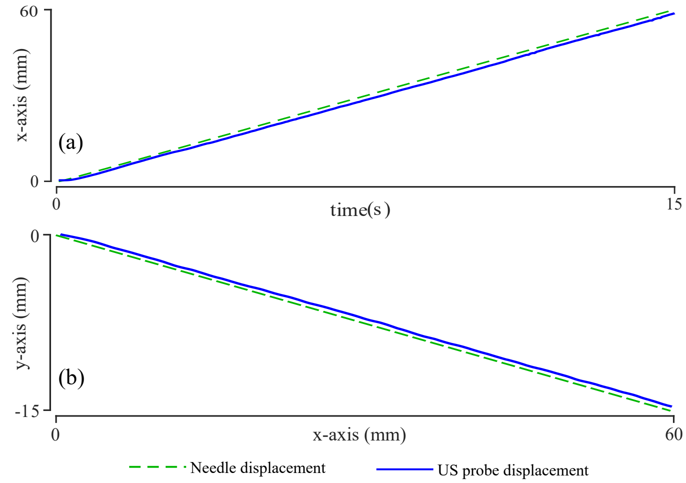

Fig. 6. Measured displacement of the needle's base and the US probe in Scenario 1 along the x-axis (a), and in Scenario 2 on the $x - y$ plane (b).

Fig. 6 shows the measured displacement of the probe and the needle. In scenario 1, the needle was displaced around 6 cm along the x-axis. As can be seen in Fig. 6(a), the US probe followed the needle movement with an average displacement error of -1.88 mm. In scenario 2, in addition to moving along the x-axis, a 1.5 cm displacement on the y-axis is added to the needle motion. Fig. 6(b) shows the displacement of the needle and the US probe in the $x - y$ plane are close, with an average error of -2.59 mm.

In scenario 3, only the needle's shaft orientation is changed, which in turn changes the needle tip position. Fig. 7(a) shows a schematic view of how the US probe tracks the needle and keeps the desired features fix. Finally, in scenario 4 the needle moved in all of its in-plane DOF, which resulted in the needle tip following a curved path. Fig. 7(b) shows the initial and final needle and US probe orientations, along with the path followed by the US probe. The sequential US images recorded at the beginning, in the middle, and at the end of the fourth test are provided in Fig. 5.

These results suggest that the proposed control system can effectively track the needle during the in-plane motion. An advantage of the proposed method is its low computational complexity. The computational time for each image sample shown in Fig. 8, is consistently less than 30 ms. This makes the proposed algorithm a good candidate for real-time clinical applications. Furthermore, the presented method only relies on US images and does not need positional information about the position of the needle's base or tip once the US probe is aligned with the needle.

V. Conclusion and Future Work

This paper presents an image-guided VS method for needle tracking based on 2D US images and real-time image moments. US-based VS has been proposed before for autonomous US imaging to a limited extent, but to the best of the author's knowledge, this paper is the first to introduce VS for 3-DOF needle tracking using 2D US images. The effectiveness of

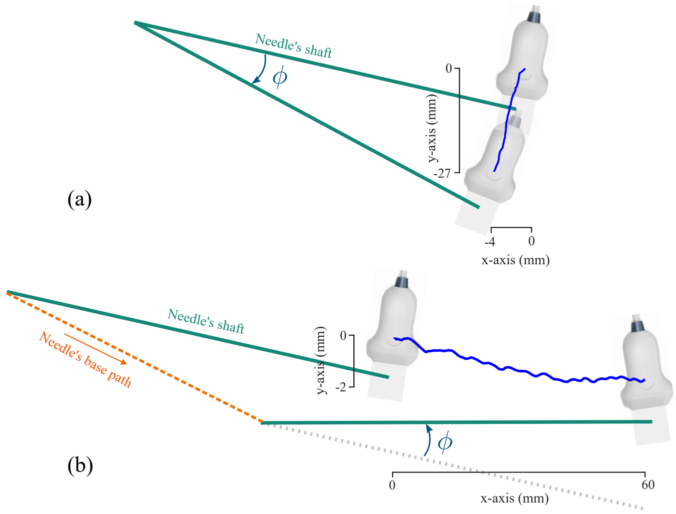

Fig. 7. Needle pose and US probe displacement measured in scenario 3 (a) and in scenario 4 (b).

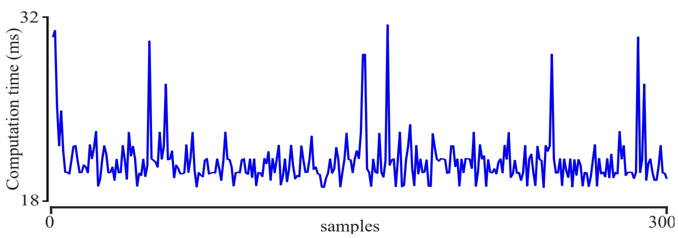

Fig. 8. Computational time for control loop sample in scenario 4. The average processing time for one sample is 23.9 ms, making the algorithm well-suited for real-time applications. Image acquisition time is not included.

the proposed method is demonstrated through experimental validation in 4 distinct scenarios. The results show that the algorithm can successfully keep the desired needle pose in the US images as the needle is steered.

Two desired features of a real-time tool-tracking algorithm are its complexity in terms of both hardware and software and its computational time. Although using 3D US imaging or electromagnetic tracking systems can provide more information regarding the needle position and its surroundings, these technologies are not accessible or applicable in many real clinical applications. On the other hand, 2D US is the current standard used in clinics and is widely accessible. Moreover, the computational time of the proposed algorithms is around 24 ms, which makes it suitable for deployment in real-time clinical settings without the need for additional resources.

Future work will focus on further improving the efficiency of the algorithm and redefining the interaction matrix to account for out-of-plane motion and to track the needle with higher accuracy. In addition, more precise image segmentation will result in a better estimation of the interaction matrix in real-time. Finally, moving away from a water tank and conducting tests on a phantom or biological tissue can provide more realistic results.

References

[1] M. Usawachintachit, S. Masic, I. E. Allen, J. Li, and T. Chi, "Adopting ultrasound guidance for prone percutaneous nephrolithotomy: evaluating the learning curve for the experienced surgeon," *Journal of endourology*, vol. 30, no. 8, pp. 856–863, 2016.

[2] J. D. Watterson, S. Soon, and K. Jana, "Access related complications during percutaneous nephrolithotomy: urology versus radiology at a single academic institution," *The Journal of urology*, vol. 176, no. 1, pp. 142–145, 2006.

[3] Y.-H. Yang, Y.-C. Wen, K.-C. Chen, and C. Chen, "Ultrasound-guided versus fluoroscopy-guided percutaneous nephrolithotomy: a systematic review and meta-analysis," *World journal of urology*, vol. 37, pp. 777–788, 2019.

[4] F. C. Ng, W. L. Yam, T. Y. B. Lim, J. K. Teo, K. K. Ng, and S. K. Lim, "Ultrasound-guided percutaneous nephrolithotomy: Advantages and limitations," *Investigative and clinical urology*, vol. 58, no. 5, pp. 346–352, 2017.

[5] D. Beiko, H. Razvi, N. Bhojani, J. Bjazevic, D. B. Bayne, D. T. Tzou, M. L. Stoller, and T. Chi, "Techniques–ultrasound-guided percutaneous nephrolithotomy: How we do it," *Canadian Urological Association Journal*, vol. 14, no. 3, p. E104, 2020.

[6] F. Ferraguti, M. Minelli, S. Farsoni, S. Bazzani, M. Bonfè, A. Vandanjon, S. Puliatti, G. Bianchi, and C. Secchi, "Augmented reality and robotic-assistance for percutaneous nephrolithotomy," *IEEE robotics and automation letters*, vol. 5, no. 3, pp. 4556–4563, 2020.

[7] Y. Tai, L. Wei, H. Zhou, J. Peng, Q. Li, F. Li, J. Zhang, and J. Shi, "Augmented-reality-driven medical simulation platform for percutaneous nephrolithotomy with cybersecurity awareness," *Int. Journal of Distributed Sensor Networks*, vol. 15, no. 4, 2019.

[8] O. Wilz, B. Kent, B. Sainsbury, and C. Rossa, "Multiobjective trajectory tracking of a flexible tool during robotic percutaneous nephrolithotomy," *IEEE Robotics and Automation Letters*, vol. 6, no. 4, pp. 8110–8117, 2021.

[9] J. Lazarus, M. Asselin, and L. Kaestner, "Optically tracked needle for ultrasound-guided percutaneous nephrolithotomy puncture: A preliminary report," *Journal of Endourology*, vol. 35, no. 12, pp. 1733–1737, 2021.

[10] S. Chen, Y. Lin, Z. Li, F. Wang, and Q. Cao, "Automatic and accurate needle detection in 2d ultrasound during robot-assisted needle insertion process," *Int. journal of computer assisted radiology and surgery*, vol. 17, no. 2, pp. 295–303, 2022.

[11] E. Ayvali and J. P. Desai, "Optical flow-based tracking of needles and needle-tip localization using circular hough transform in ultrasound images," *Annals of biomedical engineering*, vol. 43, pp. 1828–1840, 2015.

[12] R. Kojcev, B. Fuerst, O. Zettinig, J. Fotouhi, S. C. Lee, B. Frisch, R. Taylor, E. Sinibaldi, and N. Navab, "Dual-robot ultrasound-guided needle placement: closing the planning-imaging-action loop," *Int. journal of computer assisted radiology and surgery*, vol. 11, pp. 1173–1181, 2016.

[13] J. Hong, T. Dohi, M. Hashizume, K. Konishi, and N. Hata, "An ultrasound-driven needle-insertion robot for percutaneous cholecystostomy," *Physics in Medicine and Biology*, vol. 49, no. 3, pp. 441–455, 2004.

[14] F. von Haxthausen, T. Aust, H. Schwegmann, S. Böttger, F. Ernst, V. García-Vázquez, M. Kleemann, and M. Kaschwich, "Visual servoing for semi-automated 2d ultrasound scanning of peripheral arteries," in *AUTOMED-Automation in Medical Engineering*, 2020.

[15] R. Mebarki, A. Krupa, and F. Chaumette, "2-d ultrasound probe complete guidance by visual servoing using image moments," *IEEE Transactions on Robotics*, vol. 26, no. 2, pp. 296–306, 2010.

[16] C. Nadeau, A. Krupa, J. Petr, and C. Barillot, "Moments-based ultrasound visual servoing: From a mono-to multiplane approach," *IEEE Transactions on Robotics*, vol. 32, no. 6, pp. 1558–1564, 2016.

[17] H. Scholten, A. Pourtaherian, N. Mihajlovic, H. Korsten, and R. A. Bouwman, "Improving needle tip identification during ultrasound-guided procedures in anaesthetic practice," *Anaesthesia*, vol. 72, no. 7, pp. 889–904, 2017.

[18] F. von Haxthausen, S. Böttger, D. Wulff, J. Hagenah, V. García-Vázquez, and S. Ipsen, "Medical robotics for ultrasound imaging: current systems and future trends," *Current robotics reports*, vol. 2, pp. 55–71, 2021.

[19] F. Chaumette, "Image moments: a general and useful set of features for visual servoing," *IEEE Transactions on Robotics*, vol. 20, no. 4, pp. 713–723, 2004.